Article

A *Foxo1-Klf2-S1pr1-Gnai1-Rac1* signaling axis is a critical mediator of *Ostm1* regulatory network in T lymphopoiesis

Ostm1⁻ᐟ⁻ Thymus

Marie S. Mutabaruka, Monica Pata, Jean Vacher

vacherj@ircm.qc.ca

Highlights

Loss of *Ostm1* causes severe thymus hypocellularity

Ostm1 is a modulator of the T cell differentiation program from the CLPs onwards

Targeted CD2-*Ostm1* in Ostm1 null mice leads to partial rescue of DN differentiation

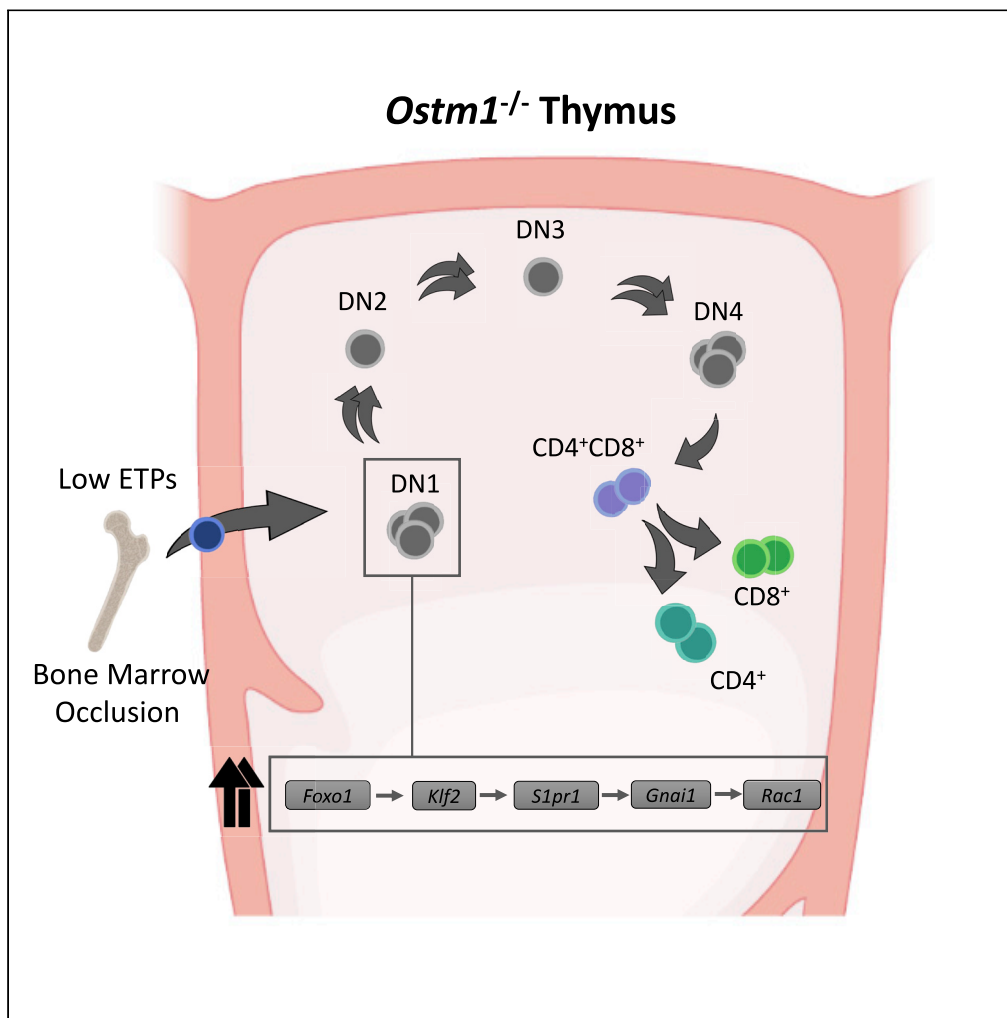*Ostm1* null DN1 transcriptome identifies a *Foxo1-Klf2-S1pr1-Rac1* signaling axis

Article

A *Foxo1-Klf2-S1pr1-Gnai1-Rac1* signaling axis is a critical mediator of *Ostm1* regulatory network in T lymphopoiesis

Marie S. Mutabaruka,[1,3] Monica Pata,[1] and Jean Vacher[1,2,3,4,*]

SUMMARY

Ostm1* mutations cause the severe form of osteopetrosis with bone marrow deficiency in humans and mice, yet a role in T cell ontogeny remains to be determined. Herein, we show that thymi of the *Ostm1*-null mice (gl/gl) from P8-to-P15 become markedly hypocellular with disturbed architecture. Analysis of gl/gl early T cell program determined a major decrease of 3-fold in bone marrow common lymphoid precursors (CLP), 35-fold in early thymic precursors (ETPs) and 100-fold in T cell double positive subpopulations. *Ostm1* ablation in T cell double negative (DN) also appears to induce fast-paced differentiation kinetics with a transitory intermediate CD44+CD25int subpopulation. Transgenic targeting *Ostm1* expression from the gl/gl DN1 population partially rescued T cell subpopulations from ETP onwards and normalized the accelerated DN differentiation, indicating a cell-autonomous role for *Ostm1*. Transcriptome of early DN1 population identified an *Ostm1* crosstalk with a *Foxo1-Klf2-S1pr1-Gnai1-Rac1* signaling axis. Our findings establish that *Ostm1* is an essential regulator of T cell ontogeny.

INTRODUCTION

Autosomal Recessive Osteopetrosis (ARO) in humans can arise from different genetic mutations (Sobacchi et al., 2013). Mutations in *OSTM1*, *TCRIG1*, and *CLCN7* responsible for ARO were first identified in the mouse (Chalhoub et al., 2003; Kornak et al., 2001; Scimeca et al., 2000). All of them are caused by absence or ineffective hematopoietic-derived osteoclast that results in poor bone resorption with obliteration of bone marrow (BM) space and frequent alteration in the hematopoietic lineage differentiation programs (Blin-Wakkach et al., 2004; Frattini et al., 2000; Pata et al., 2008). Among the ARO, the *OSTM1* spontaneous mutations cause the most devastating form of the disease with severely reduced marrow and neurologic defects that cause death in infancy (Maranda et al., 2008; Ott et al., 2013; Quarello et al., 2004). Clinical studies in ARO patients reported increased susceptibility to infections that were linked to weak immunological responses from defective BM (Guerrini et al., 2008; Pangrazio et al., 2012; Reeves et al., 1979). Accordingly, patients that underwent BM transplantation displayed correction of the immunological defects in addition to osteopetrosis (Mazzolari et al., 2009; Orchard et al., 2015).

Functional bone physiology was shown to be critical for normal hematopoietic differentiation. The hematopoietic and bone cells not only share the same microenvironment but also crosstalk through highly dependent cellular and paracrine interactions (Takayanagi et al., 2000). In humans and in mice, the mature osteoclast is essential for both bone physiology and several hematopoietic functions. A role for mature osteoclasts in production of the hematopoietic stem cell (HSC) niches via bone remodeling is of high importance in supporting the HSC cell population (Lymperi et al., 2011). Osteoclasts were also reported to promote mobilization of multipotent hematopoietic precursors that are committed into myeloid and lymphoid lineages (Kollet et al., 2006; Mansour et al., 2012).

In the mouse, the *Ostm1* null gl/gl osteopetrotic phenotype is characterized by inactive and enlarged osteoclasts, reduced BM and early death by ∼3-week of age (Rajapurohitam et al., 2001). Ostm1 is implicated in intracellular trafficking and dispersion of cargos on microtubules that is an essential function for bone resorption (Pandruvada et al., 2016; Pata and Vacher, 2018). A key role of *Ostm1* in osteoclast lineage was inferred from the full rescue of the gl/gl osteopetrotic phenotype by targeting *Ostm1* with the PU-1 regulatory regions that simultaneously corrected the hematopoietic defects (Pata et al., 2008). However,

the aging osteopetrotic-rescued gl/gl mice develop acute neurodegeneration with impaired neuronal autophagy overtime, as observed in humans (Héraud et al., 2014). At present, *Ostm1* thus plays two essential physiologic functions in at least the osteoclastic and neuronal lineages. Ostm1 may also contribute to other lineages because gl/gl mice display anemia and hematopoietic anomalies in lymphoid cells. Besides, evidence for a specific role of *Ostm1* or ARO mutations in the T cell lymphoid lineage, whether directly or indirectly, remains to be determined.

T cell lymphoid lineage originates from BM HSC and CLP. Commitment to the lymphopoietic program is instructed by a series of sequential cellular and signaling events that is initiated by mobilization of marrow lymphoid progenitors that seed the thymus followed by engagement into the T cell lineage (Cyster, 2009; Gossens et al., 2009; Shah and Zúñiga-Pflucker, 2014; Yokota, 2006; Zúñiga-Pflucker, 2009). In the thymus, precursors CD4⁻CD8⁻ referred to as double negative (DN) consist of four immature subsets based on expression of CD25 and CD44. The DN1 (CD44$^+$CD25$^-$) migrate from the cortico-medullary junction to the subcapsular region of the thymus and differentiate into DN2 (CD44$^+$CD25$^+$) and DN3 (CD44$^-$CD25$^+$) subsets, which following TCR-β gene rearrangement give rise to the DN4 (CD44$^-$CD25$^-$) cell subset. Subsequently, DN4 cells that progress to double positive (DP) CD4$^+$CD8$^+$ stages in the outer cortex and in the medulla give rise to single positive (SP) CD4$^+$ or CD8$^+$ (Bleul et al., 2006; Misslitz et al., 2004). The intrathymic differentiation program relies on specific molecular signals, such as Notch, which are essential for survival, proliferation, and differentiation (Bhandoola et al., 2007; Mohtashami and Zúñiga-Pflucker, 2006). The reduced BM in ARO patients raised the questions whether in *Ostm1* null gl/gl mice production, mobilization of BM early T precursors and/or ETPs thymic differentiation program potential could be altered.

The present study determined that the loss of *Ostm1* in gl/gl mice lead to thymic cellular depletion and altered architecture specifically from the second wave of thymic colonization. Our findings demonstrate that *Ostm1* can regulate not only BM precursor and thymic ETPs cell population but also early T cell differentiation kinetics and distinct cell population stages. By *in vivo* transgenic complementation analysis in the DN1 stage onward, the rescued gl/gl T cell differentiation program defined at least a cell-autonomous role for *Ostm1* within the DN1 to SP stages. We further characterized a crosstalk between *Ostm1* and a regulatory *Foxo1-Klf2-S1pr1-Gnai-Rac1* signaling axis essential in T cell motility, differentiation, and proliferation for lineage homeostasis.

RESULTS

Ostm1 deficiency affects thymus architecture and T cell subpopulations

Quantitative expression of *Ostm1* was first evaluated in immune cells and showed comparable levels in T, B, NK, bone marrow macrophage cell (BMMC), and peritoneal macrophages (MAC) of enriched hematopoietic cells (Figure S1). To determine *Ostm1* expression pattern in individual T cell subpopulations, sorted wild type thymus T-cells from the early precursors ETP, DN1 to DN4, DP, and SP populations, were assessed by quantitative PCR (qPCR) (Figure 1A). Of interest, *Ostm1* expression is detected in all T cell subpopulations. ETP and DN4 expressed ∼5-fold higher *Ostm1* levels relative to DN1, whereas the DP cell population is further increased to ∼25-fold. *Ostm1* expression then decreased in SP T cells to levels slightly above those detected for total DN cell population (Figure 1A). The wide range of expression levels show marked differential regulation of *Ostm1* in these cell subpopulations.

We then interrogated the role of *Ostm1* in the gl/gl thymus and T cell differentiation program. Quantification of gl/gl circulating lymphocytes revealed an important depletion by 5-fold relative to wild type, of which ∼40% are T cells indicating a markedly affected T lymphocyte population (Table S1A). In particular, quantification of circulating gl/gl CD4$^+$ and CD8$^+$ T cells showed a major reduction compared to wild type (Table S1B). Although the gl/gl mice exhibit severe growth delay at postnatal day 21 (P21), thymi show a further reduction in size by ∼2-fold (Figure 1B). Longitudinal analysis revealed that in gl/gl mice at P3, the cellularity of thymus is comparable to controls (Figure 1C). Noticeably from P15 onward, gl/gl thymus shows a ∼10-fold decrease in absolute cell number (Figure 1C). We then investigated this hypocellularity by histology from P8 to P21 that displays progressive abnormal architecture with significant fewer cells in cortex and a disorganized cortico-medullary junction at P21 (Figure 1D), inferring that *Ostm1* is a critical modulator of lymphopoietic subpopulations.

Analysis of the T cell subpopulations at P21 shows that the gl/gl immature DN cells are significantly decreased by ∼3-fold (Figure 1E). Strikingly, the DP population, that normally has the highest *Ostm1*
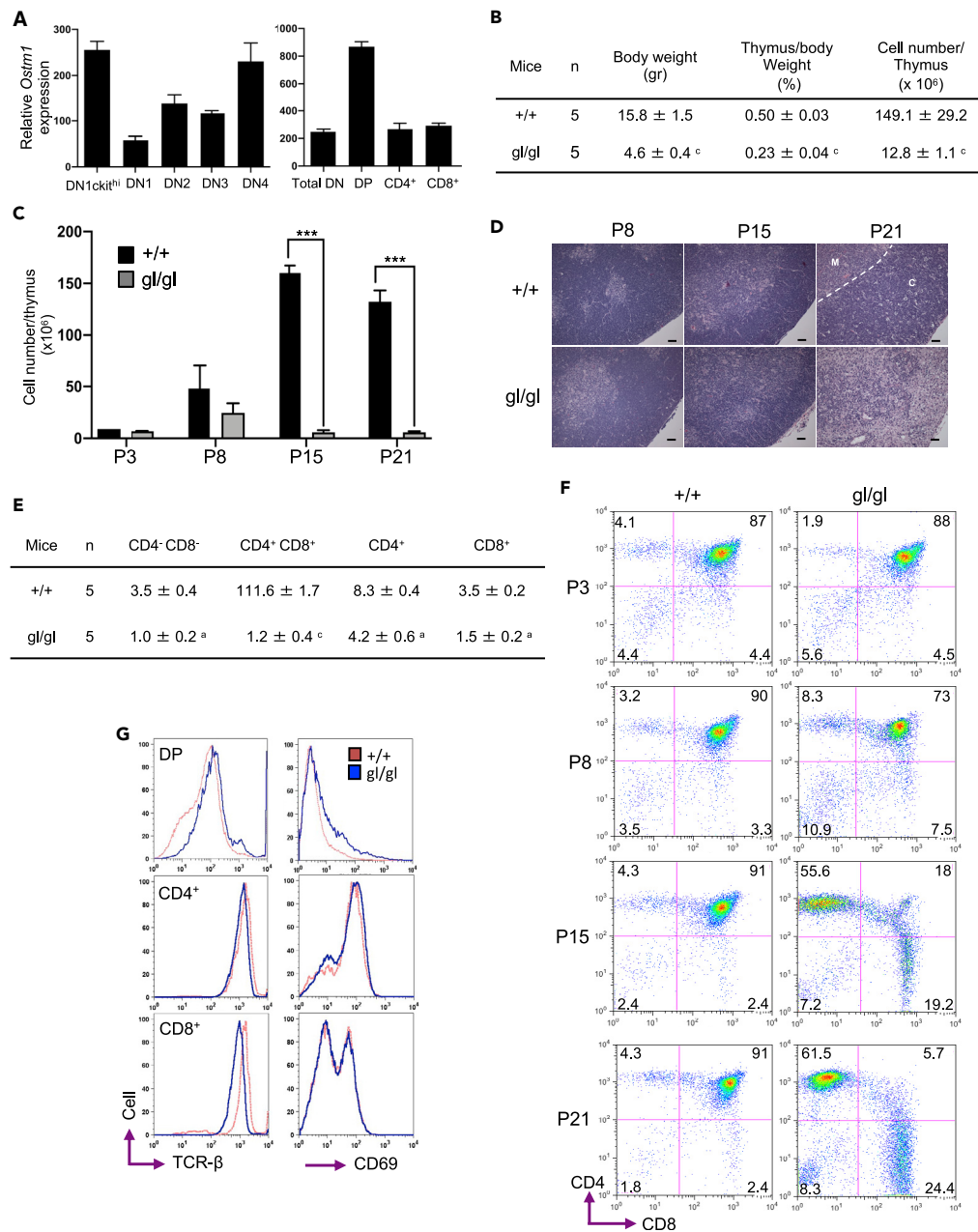
Figure 1. gl/gl thymic phenotype develops temporal-dependent abnormal architecture, low cellularity, and defective T cell distribution

(A) Real-time quantitative *Ostm1* expression in sorted wild type (+/+) T cell populations from DN1 c-Kit^{hi}/ETP to DN4 (left panel) and DP to mature SP CD4^{+} or CD8^{+} (right panel) relative to S16 as internal control (n = 4). Data are represented as mean ± SEM.

(B) gl/gl thymus, body weight, and their relative ratio as well as thymic cellularity quantified as mean × 10[6] ± SEM compared to wild type controls (+/+). [c] p < 0.001.

(C) Longitudinal age-dependent quantification of thymus cellularity for gl/gl and controls (+/+) thymi (n = 3). ***p < 0.001. Data are represented as mean ± SEM.

(D) Representative thymus sections from control (+/+) and gl/gl mice at P8, P15, and P21. Altered thymic architecture from gl/gl is detected by P15. Staining with H&E; C: Cortex; M: Medulla. (Scale bar: 50 μm).

(E) Analysis of T cell distribution in control (+/+) and gl/gl thymi. Data are expressed as the means of cell number x 10[6] ± SEM. (n = 5). [a] p < 0.05, [c] p < 0.001.

Figure 1. *Continued*

(F) Longitudinal quantification of CD4$^+$ CD8$^+$ positive cell distribution in control (+/+) and gl/gl thymus at P3, P8, P15, and P21 show severe depletion of DP in gl/gl from P15. Data are representative of three independent FACS experiments from age-matched littermates.

(G) Representative thymi expression profile of TCR-β and CD69 in DP and in SP CD4$^+$ or CD8$^+$ populations from gl/gl and control (+/+) at P21.

expression, is markedly reduced in gl/gl thymus by almost ~100-fold, whereas the number of more mature SP CD4$^+$ or CD8$^+$ T cells is reduced by ~2-fold (Figure 1E). Considering gl/gl thymus cellularity, the relative number of DN, DP, and SP is even further decreased compared to controls (Figure 1E). Longitudinal gl/gl DP and SP populations distribution detected no significant difference at P3 and P8 (Figure 1F). However, from P15 onward, a major depletion of the DP gl/gl population is measured compared to controls, reaching ~6% at P21 (Figure 1F). Concurrently, the T cell subpopulation distribution exhibits a relatively marked increase in mature CD4$^+$ and CD8$^+$ but in absolute cell number still below those quantified in controls. To characterize the gl/gl SP population and even the few DP cells, analysis of specific markers of differentiation and activation/maturation, TCR-β^{hi} or CD69^{hi} was performed and show comparable distribution pattern in gl/gl and controls (Figure 1G), indicating that *Ostm1* does not modulate TCR gene rearrangement within this differentiation process.

Ostm1 does not affect distribution of T cell subpopulations in extrathymic organs

Because mature SP cells from a positively selected DP population migrate into peripheral lymphoid tissues to mediate immune response (Weinreich and Hogquist, 2008), the spleen and lymph nodes of gl/gl and controls were examined. The gl/gl spleen cellularity is significantly reduced by ~3-fold relative to controls (Figure 2A). From FACS analysis, the proportion of mature CD4$^+$ or CD8$^+$ in the gl/gl spleen appears comparable to controls. The percentage of naïve T cell population (CD62L$^+$CD44^{lo}) in the mature CD4$^+$ or CD8$^+$ fractions of gl/gl spleen is at least equivalent or slightly higher than in controls (Figure 2B). In lymph nodes, the percentage of naive CD4$^+$ or CD8$^+$ T cell population is similar in both gl/gl and controls (Figure 2C). The loss of *Ostm1* does not seem to affect the cell subpopulation distribution in lymphoid organs, but the reduced cell number in the spleen could result from a deficit of earlier SP subpopulation.

Ostm1 plays distinct regulatory roles on thymic ETP and DN T cell differentiation

To investigate the cellular mechanism leading to DP cell depletion, we monitored the earlier T cell differentiation in gl/gl thymi. At P21, the number of ETPs Lineage$^-$ Sca-1$^+$ CD44$^+$c-kit^{hi} population is decreased by ~35-fold in gl/gl (Figure 3A), inferring a major role of *Ostm1* on earlier marrow egression, thymic homing, and/or on cell differentiation rate in successive stages. The T cell precursor differentiation potential was then monitored from DN1 to DN4 cell populations within the gl/gl thymus at P8, P15, and P21. As shown in Figure 3B, DN T cell differentiation pattern at P8 is similar in gl/gl and controls. At P15, the DN2 and DN3 gl/gl subpopulations are markedly reduced, whereas the DN1 is not decreased or even relatively increased, suggesting a pause or delay in DN1 differentiation. At P21, the proportion of gl/gl DN1 cell subpopulation becomes comparable to controls; nonetheless, the DN2 and DN3 cell subpopulations remain substantially decreased by ~10-fold (Figure 3B). Interestingly, the presence of a distinct intermediate subpopulation (CD44$^+$CD25^{int}) at P15 and P21 is clearly distinguishable and specific for gl/gl thymus (Figure 3B), suggesting that *Ostm1* modulate CD25/IL2Rα expression or DN differentiation. These results show that *Ostm1* plays a key temporal-dependent role during or before the ETP and at the DN1-DN2 stage that could depend on thymic stromal microenvironment or on *Ostm1* intrinsic function in T cell differentiation.

Ostm1 regulates kinetic of T cell differentiation program *ex vivo*

To determine whether the altered differentiation profile results from partial inhibition and/or from accelerated rate of differentiation, we assessed *Ostm1* role in T cell precursor differentiation independently of the thymic microenvironment. Cocultures of ETPs from gl/gl and controls with notch-responsive OP9-DL4 stromal cells (Mohtashami et al., 2013) were monitored at different time points. Up to 8 days in culture, the DN subpopulations of gl/gl show a similar distribution as controls (Figure 3C). By 15 days, a marked decrease in the gl/gl DN2 subset was detected concomitant with major increase in DN4. At day 20, the proportion of both DN2 and DN3 subpopulations in gl/gl are considerably reduced relative to controls associated with a further increase in DN4 cell population (Figure 3C). This temporal distribution pattern is consistent with an accelerated differentiation process of gl/gl ETPs, independently from an *in vivo* pressure of differentiation. In addition, the gl/gl DP subset had a 2-fold
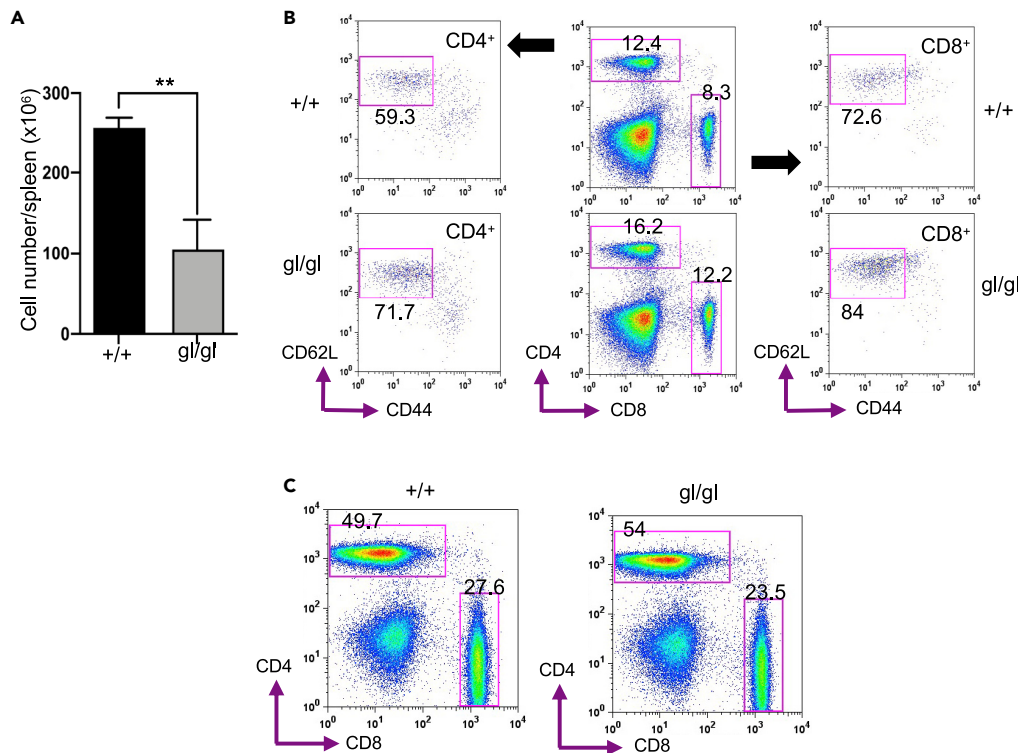
Figure 2. Loss of *Ostm1* on extrathymic T cell differentiation

(A) Spleen total cell number is quantified at P21. Cellularity is significantly reduced in gl/gl compared with controls (+/+), expressed as mean x 10^6 ± SEM (n = 4). **p < 0.01.

(B) Representative spleen cellular distribution of mature SP CD4$^+$ or CD8$^+$, and related naïve T cells fractions CD62L$^+$CD44$^+$ within control (+/+) and gl/gl at P21 (n = 3).

(C) Representative lymph node distribution of mature SP CD4$^+$ or CD8$^+$ harvested from control (+/+) and gl/gl mice at P21 (n = 3).

increase in comparison to controls at day 15 and remained elevated at day 20 (Figure 3D), indicating that gl/gl ETPs has the potential to differentiate and respond efficiently to notch signaling. Such an increase in gl/gl DP subpopulation is consistent with rapid ETP differentiation both *ex vivo* and *in vivo* and suggests that *in vivo* DP undergoes a swift differentiation-induced mechanism likely in response to SP demand. These *ex vivo* with the *in vivo* analyses concomitantly point to a direct regulatory role of *Ostm1* in the kinetic of T cell subpopulation differentiation.

Ostm1 autonomous role in T cell differentiation through transgenic complementation

To assess whether *Ostm1* role in T cell subpopulations is independent of other hematopoietic cells or hematopoietic organ environments *in vivo*, we targeted expression of *Ostm1* V5 tagged with the human hCD2 cassette, active in T cell ontogeny initiating from the DN1 subset to peripheral lymphocytes (Brodeur et al., 2009; de Boer et al., 2003). Two transgenic hCD2-V5-*Ostm1* mouse lines (TR777, TR805) were established containing ~13 and 5 copies of the transgene (Figure 4A). Transgene quantitative expression is specifically detected for both lines in hematopoietic tissues, thymus, and spleen, in approximately similar ratio as the transgene copy number (Figure 4B). Consistently, CD2-*Ostm1* transgene displays a comparable protein expression pattern on immunoblots (V5-Ostm1) (Figure 4C). *Ostm1* transgene quantitative expression in sorted thymic subpopulations exhibits analogous expression profile to endogenous *Ostm1*. High CD2-*Ostm1* expression levels were quantified in the ETP, DN4, and DP subpopulations relative to DN1 (Figure 4D). CD2-*Ostm1* transgenic thymi also display similar size, cell number, and architecture as in controls (Figure 4E).

The *in vivo* role of *Ostm1* in T cell ontogeny was investigated in gl/gl progenies by intercrosses. Although the body weight of CD2-*Ostm1* gl/gl (gl/gl TR, transgenic) was reduced relative to control mice (+/+ TR), the thymus to body weight ratio was almost normalized at P21 (Table S1C). Consistently, gl/gl TR thymi exhibit at P21 a
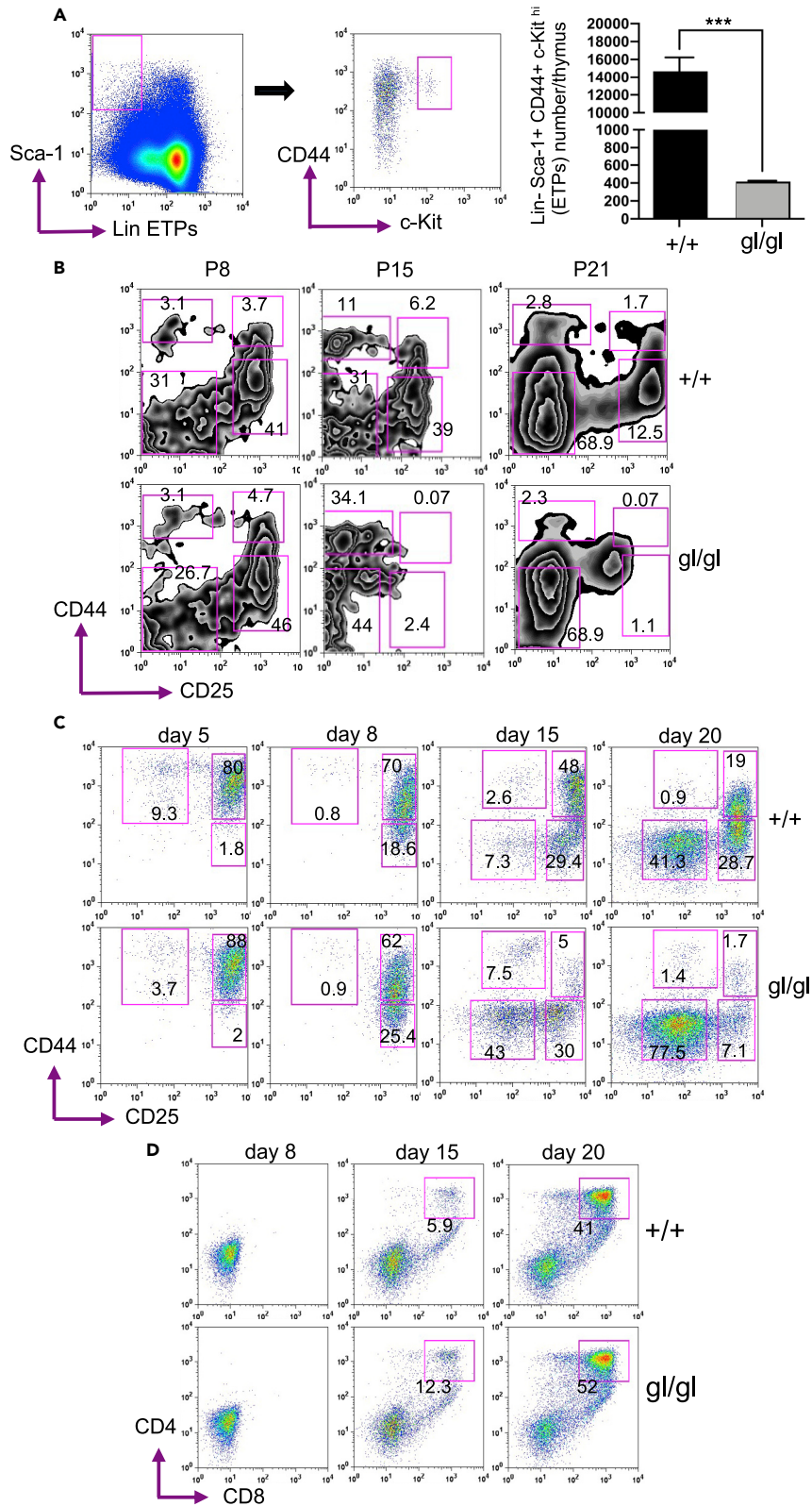
A

B

P8   P15   P21

+/+

gl/gl

CD44 / CD25

C

day 5   day 8   day 15   day 20

+/+

gl/gl

CD44 / CD25

D

day 8   day 15   day 20

+/+

gl/gl

CD4 / CD8

Figure 3. gl/gl ETP depletion and *in vivo* and *ex vivo* DN T cell differentiation

(A) Early T precursors ETP (Lin⁻Sca1⁺CD44⁺cKit^hi) cell number in thymus is markedly reduced in gl/gl compared with control (+/+) thymi at P21, expressed as mean ± SEM (n = 3) ***p < 0.001.

(B) Representative *in vivo* longitudinal analysis of DN1, DN2, DN3, and DN4 T cell subpopulations quantified in age-matched control (+/+) and gl/gl littermates at P8, P15, and P21 from Lin⁻Sca1⁺CD44⁺cKit^hi. Evidence of an intermediate subpopulation CD44⁺CD25^int is readily detectable in gl/gl at P15 and P21 (n = 6).

(C) *Ex vivo* longitudinal analysis of ETPs (Lin⁻Sca1⁺CD44⁺cKit^hi) differentiation profile in OP9-DL4 coculture assays for 5, 8, 15, and 20 days. Kinetic of DN differentiation by analysis of CD44 and CD25 subpopulations is accelerated in gl/gl relative to controls (+/+) at day 20. Data are representative of three independent FACS experiments.

(D) Quantification of CD4⁺ CD8⁺ positive cell distribution from the *ex vivo* longitudinal analysis in gl/gl and controls (+/+) at day 8, 15, and 20 in coculture.

significant ~5-fold increase in total cell number (Figure 4E) in comparison to gl/gl. Peripheral blood cell parameters from both gl/gl TR and control mice (+/+ TR) and without the transgene (+/+ NT, non-transgenic) show significantly improved white blood cells (WBC) and lymphocytes in comparison to gl/gl but does not reach control levels (Table S1A). In fact, the gl/gl TR T lymphocyte population is likely normalized considering that T cells represent ~20% of WBC or ~40% lymphocytes. Further, the CD2-*Ostm1* T cell lineage transgene specificity in gl/gl mice is supported by non-rescue red blood cell (RBC), hematocrit, or hemoglobin values (Table S1A).

Remarkably, CD2-*Ostm1* expression in gl/gl thymus corrected the distribution of DN T cell subpopulations at P21 (Figure 4F) similar to the wild type controls (Figure 3B). Particularly, the differentiation profile at the DN1/DN2 transition stage is significantly improved for both transgenic lines compared to gl/gl, correcting the DN rapid differentiation kinetic (Figure 4F). Notably, the gl/gl thymic intermediate subpopulation CD44⁺CD25^int is no longer detectable; rather, an unambiguous CD44⁺CD25⁺ subpopulation is distinguished upon expression of CD2-*Ostm1*. Significantly, the severely affected DP T cell subpopulation and mature CD4⁺ and CD8⁺ distribution in gl/gl thymus are virtually rescued in gl/gl TR (Figures 4F and 1F), consistent with transgene expression in these cell subsets (Figure 4D). Hence, *Ostm1* achieves essential roles in the T cell subpopulations differentiation process from the DN stage onward.

Because CD2-*Ostm1* targets the DN population onward, we determined whether the gl/gl ETPs depletion results solely from the altered successive T cell subpopulation stages. Quantification of the very early T cell progenitors in the thymus of gl/gl TR at P21 detected a major ~10 fold increase compared to gl/gl (Figure 4G). This partial rescue, due to correction of the differentiation rate in successive stages, likely results in reduced request of ETP differentiation. Because the ETPs still display a significantly ~3-fold lower cell pool than controls, it points to a role of Ostm1 before or at this stage of T cell lineage commitment. To address this point, LSK and CLP cell populations that give rise to ETP were evaluated in bone marrow. Despite marrow hypocellularity, the frequency of LSK cell populations in gl/gl and gl/gl TR are similar to controls; however, in absolute number, this population is reduced (Figure 4H). The frequency of CLP population in contrast is markedly decreased in gl/gl TR and gl/gl relative to controls, suggesting that *Ostm1* play a key role in lymphoid cell precursor proliferation, survival, or self-renewal. Hence, *Ostm1* seems a critical modulator of the very early T cell commitment program.

Ostm1 rescues T cell differentiation program independently of the osteoclast lineage

Because the T cell lineage was shown to crosstalk with the osteoclast lineage, we monitored osteoclast function and bone status in gl/gl TR mice. Mature osteoclast cell population was analyzed from cultured splenic hematopoietic progenitors. Mature-multinucleated osteoclasts from gl/gl TR detected by Tartrate Acid Phosphatase (TRAP) staining are oversized similarly to enlarged gl/gl osteoclasts (Figure 4I). Osteoclast functional properties were then characterized by scanning bone femurs with X-rays. As shown in Figure 4J, femur size of gl/gl TR are not only, as in gl/gl, significantly shorter but also of similar increase in bone density relative to controls, providing evidence that the osteoclasts are nonfunctional and responsible for defective marrow cellularity. This phenotype provides evidence that *Ostm1* does not interfere in the T cell osteoclast-crosstalk mechanism but functions independently within the T and osteoclast lineages.

Ostm1 transcriptome signature in DN1 thymocytes

To decipher *Ostm1* molecular regulation during the altered thymopoietic DN1 to DN2 transition phase, transcriptomic profiles of enriched DN1 cell subpopulation were analyzed. RNA seq of DN1 cells from gl/gl NT, gl/gl TR, and control (+/+ NT) thymi were quantified as fragment per kilobase of transcripts per million fragments mapped (FPKM) aligned to specific genes that correspond to the number of transcripts in total sample (Figure 5A). DN1 from gl/gl TR and controls show relatively similar transcript
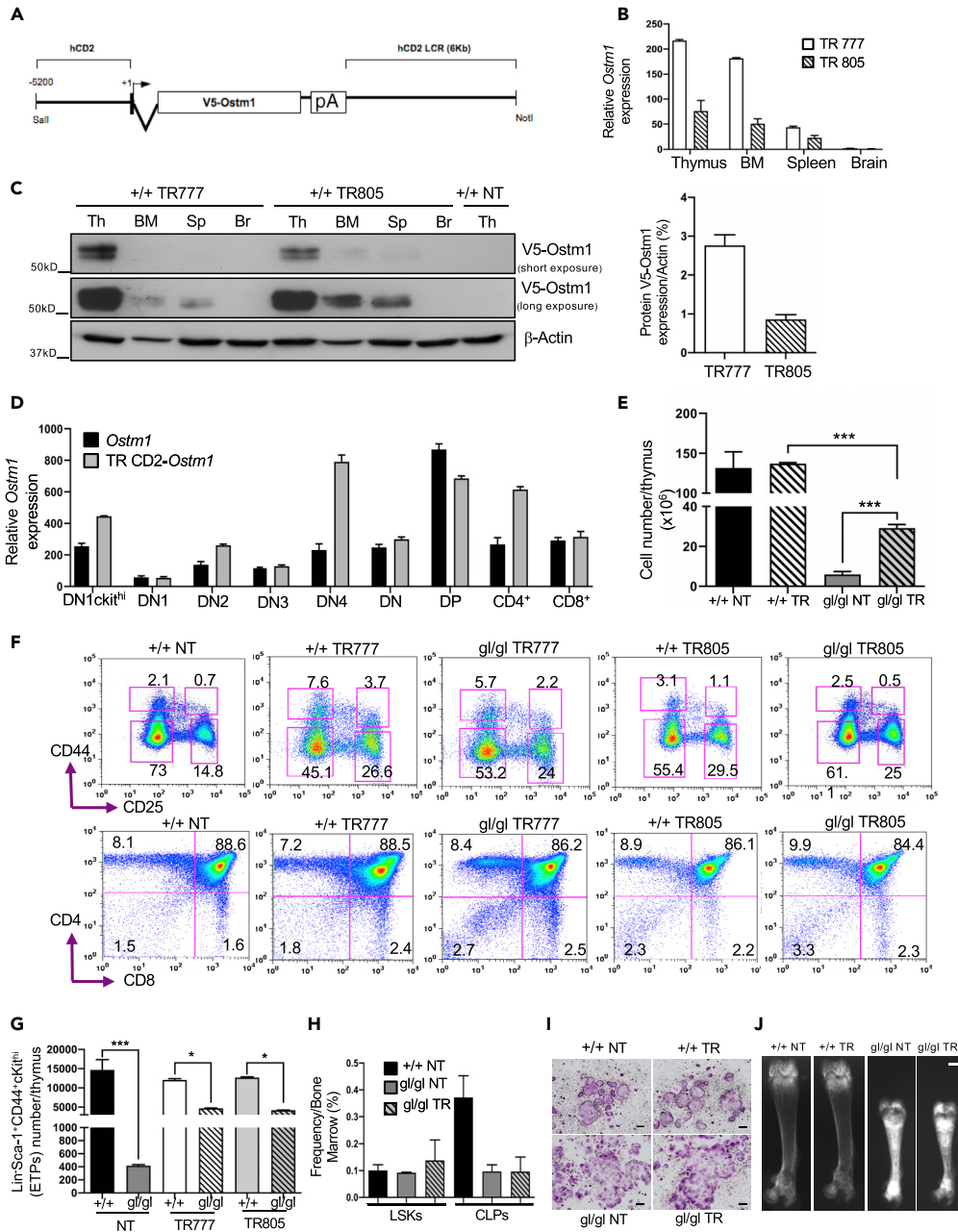
Figure 4. Rescue of gl/gl T cell differentiation in CD2-Ostm1 transgenic mice

(A) Schematic representation of the CD2-Ostm1 transgene that consist of the 5.2 kb human hCD2 promoter sequence upstream of the V5-tagged Ostm1 cDNA sequence followed by polyA and the 6 kb hCD2 locus control region (LCR).

(B) CD2-Ostm1 transgene expression analysis by real-time quantitative PCR on tissues from transgenic lines 777 and 805 relative to S16 internal control, (n = 3). Data are represented as mean ± SEM.

(C) Representative protein analysis by Western blot on different tissues of the transgenic V5-Ostm1 lines compared to +/+ non-transgenic (+/+ NT) controls (n = 4). Histogram (right panel) shows quantification of V5-Ostm1 protein expression in thymus (n = 4/genotype). Data are represented as mean ± SEM.

(D) Real-time quantitative CD2-Ostm1 transgene expression relative to endogenous Ostm1 of sorted wild type T cell populations from DN1 c-Kit^{hi}/ETP to DN4 and DP to mature SP CD4^{+} or CD8^{+} normalized to S16 as internal control. Data are represented as mean ± SEM.

(E) Total thymic cellularity in gl/gl TR and gl/gl NT mice and age-matched control mice (+/+ NT, +/+ TR) at P21 (n = 5). ***p < 0.001. Data are represented as mean ± SEM.

Figure 4. *Continued*

(F) Representative experiment of differentiation profiles from immature DN1 to DN4 stages (n = 6), DP CD4$^+$/CD8$^+$ to mature SP CD4$^+$ or CD8$^+$ in gl/gl TR, +/+ TR and control (+/+ NT) thymi (n = 10).

(G) Thymic total ETPs (Lin$^-$Sca1$^+$CD44$^+$c-Kit^{hi}) cell number in gl/gl NT compared to control (+/+ NT) and of gl/gl TR compared to the respective transgenic line TR at P21 (n = 3). *p < 0.05; ***p < 0.001. Data are represented as mean ± SEM.

(H) Frequency of BM multipotent precursors (LSKs or Lin$^-$Sca-1$^+$CD44$^+$ckit$^+$IL7R$^-$) and common lymphoid precursors (CLPs or Lin$^-$Sca-1$^+$CD44$^+$cKit$^+$IL7R$^+$) populations of gl/gl NT, gl/gl TR and controls (+/+), mice (n = 2). Data are represented as mean ± SEM.

(I) *Ex-vivo* analysis of osteoclast differentiation from controls (+/+ NT, +/+ TR), gl/gl NT, and gl/gl TR splenic hematopoietic progenitors carried out in presence of M-CSF and RANKL. Mature-multinucleated osteoclasts of gl/gl NT and gl/gl TR are enlarged as revealed with TRAP staining. (Scale bar: 200 μm).

(J) Representative X-ray scan analysis of controls (+/+ NT, +/+ TR), gl/gl NT, and gl/gl TR femurs at P21 (n = 5). (Scale bar: 1 mm).

distribution whereas DN1 gl/gl transcriptome has an important number of outlier transcripts (Figures 5A and 5B). Within DN1 sorted cells of gl/gl in comparison to gl/gl TR and controls, we identified 205 and 146 differentially expressed genes (DEGs) respectively (Figure 5C). Heat map analysis of DEGs within the DN1 gl/gl TR and control determined similar downregulated and upregulated genes that contrast with the expression signature of DN1 gl/gl (Figures 5D and 5E).

To identify biological processes or signaling pathways modulated by Ostm1, DEGs within DN1 gl/gl transcripts were subjected to DAVID, IPA, and *GSEA* bioinformatics processing (Tables S2A and S2B). Significant variations in 11 biological functions and 5 signaling pathways (Tables S3A and S3B) were detected within DN1 gl/gl transcriptome in comparison to DN1 control and gl/gl TR. Of all the biological processes that were apparently affected, cell migration/motility, differentiation, immune cell trafficking/chemotaxis, and hematopoietic organ development were decisive in T cell differentiation program.

Ostm1 crosstalk with *Foxo1-Klf2-S1pr1-Gnai1-Rac1* signaling axis in T cell precursors

To uncover Ostm1 molecular mechanism during early T cell ontogeny, analysis of the most important upregulated gene sets by Gene ontology terms (Go terms) pointed to genes implicated in lymphoid differentiation, migration, and development (Figure 6A). We focused on quantification by GSEA of cell migration associated-genes and determined a significant normalized enrichment score (NES) of 1.42 for DN1 gl/gl NT versus DN1 +/+ NT and of 1.77 relative to gl/gl TR profiles (Figure 6B). We then investigated the highest differentially expressed migration associated-genes using a heat map at the individual gene level for DN1 gl/gl NT, +/+ NT, and gl/gl TR (Figure 6C). Two related genes in a signaling pathway, known to be crucial in immune cell migration and differentiation (Dorsam et al., 2003), were detected as the most DEGs in DN1 gl/gl when compared to either control DN1 or gl/gl TR. Both the Sphingosine-1-phosphate receptor 1 gene (*S1pr1*) that encodes the G protein-coupled receptor (GPCR) S1P$_1$, and its downstream effector the small G protein Rac GTPase 1 gene (*Rac1*) were strongly upregulated as validated by qPCR in DN1 gl/gl NT cell subpopulation (Figure 6D). In the DN1 gl/gl TR population, *S1pr1* and *Rac1* gene expression are normalized, suggesting that *Ostm1* regulates cell trafficking and mobility or even egression of thymic progenitors (Figure 6D).

Analysis of DN1 transcriptome gl/gl profiles for the *S1pr1-Rac1* signaling pathway identified that two direct upstream transcriptional activators of the S1P$_1$ receptor, *Foxo1* and *Klf2*, within the cascade (Bai et al., 2007; Carlson et al., 2006) are substantially upregulated as confirmed by qPCR (Figure 6E). Consistently, targets of *Foxo1* and of *Klf2*, the cytokine receptor *IL7r* and the chemokine receptor *Ccr7* genes (Kerdiles et al., 2009) display increased transcripts in DN1 gl/gl NT, compatible with regulation of intrathymic cell motility. Interestingly, the Gαi subunit, a direct partner of S1P$_1$ and upstream activator of Rac1 (Xiao et al., 2019), was also shown to be upregulated in the transcriptome (Figure 6F). To determine whether Ostm1 could also regulate S1P levels and interaction with *S1pr1*, expression of S1P modulators was monitored in the DN1 gl/gl NT, +/+NT and gl/gl TR cell subpopulations. In fact, expression of Sphingosine kinase 2 (*Sphk2*), Sphingosine-1 transporter (*Spns2*), Sphingosine-1-phosphatase lyase (*Sgpl1*), and Sphingosine-1-phosphate phosphatase 2 (*Sgpp1*) remain unchanged (Figure 6D), suggesting that *Ostm1* specifically modulates the expression of *S1pr1* independently of S1P modulators. Collectively, a direct transcriptional cascade *Foxo1*, *Klf2*, *S1pr1*, *Gnai1*, and *Rac1* in DN cells uncovered by loss of *Ostm1* revealed that *Ostm1* is a critical negative transcriptional modulator of this signaling axis (Figure 6G) toward regulation of the T cell progenitor differentiation program.

Figure 5. Analysis of gl/gl DN1 lymphocytes transcriptome signature

(A) Identification of differentially expressed transcripts in sorted DN1 (Lin⁻CD44⁺CD25⁻) from gl/gl TR as opposed to gl/gl NT (red circles) and to wild type (+/+ NT) controls.

(B) Matrix representing the distant location of outlier DN1 transcripts in gl/gl NT in comparison to wild type (+/+ NT) and gl/gl TR.
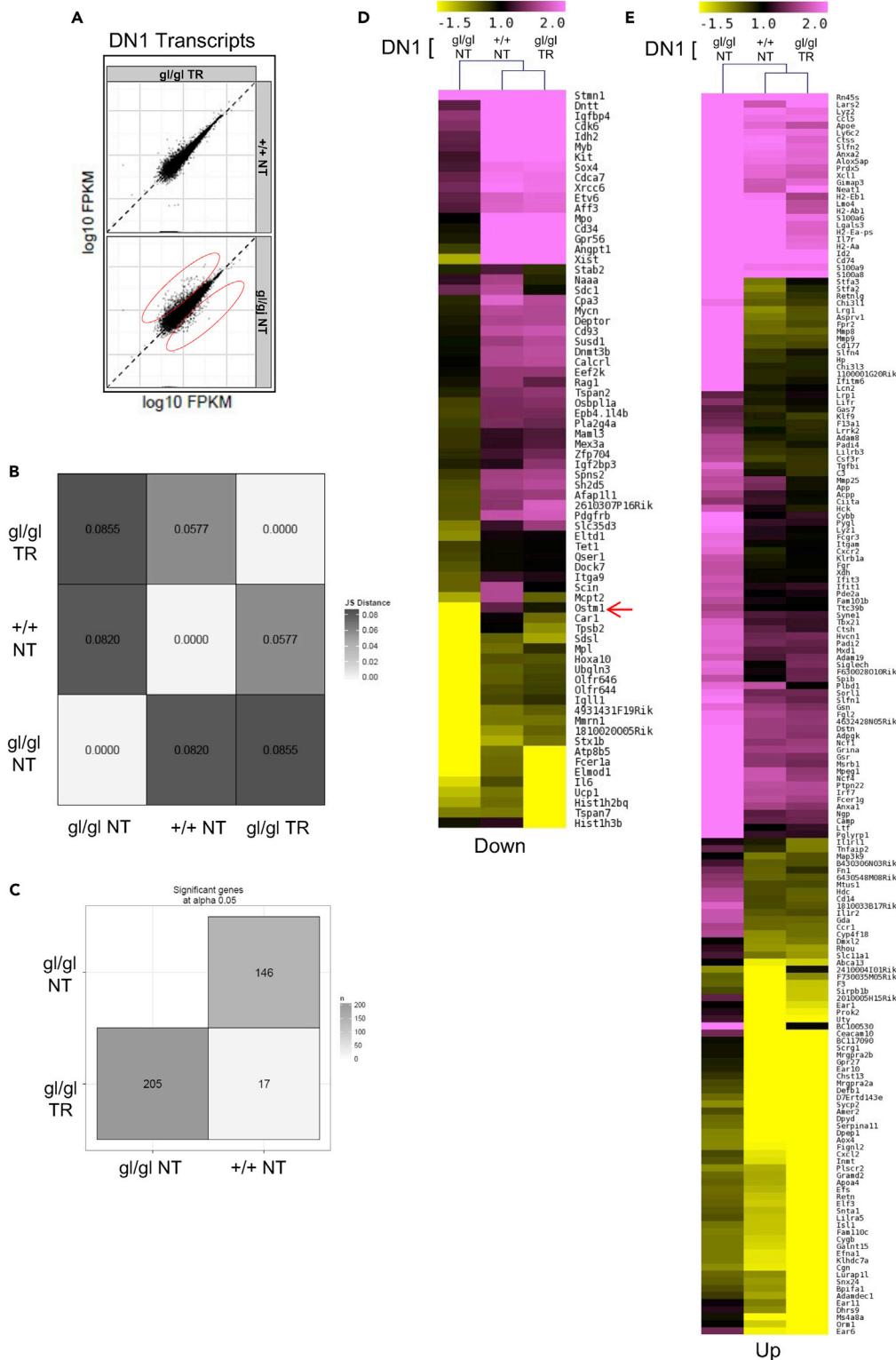
Figure 5. *Continued*

(C) Sig matrix representation of the differentially expressed gene numbers within sorted DN1 gl/gl NT cell populations compared to DN1 wild type (+/+ NT) and gl/gl TR.

(D) Heat map representation of the top downregulated genes across DN1 gl/gl NT transcripts compared to DN1 wild type (+/+ NT) and gl/gl TR.

(E) Heat map representation of top upregulated genes across DN1 gl/gl NT transcripts compared to DN1 wild type (+/+ NT) and gl/gl TR.

DISCUSSION

Our study defines diverse biological functions for *Ostm1* in T cell ontogeny detectable from the second wave of thymic cell colonization. The *Ostm1* null gl/gl mice show a defect from the early medullary multipotent precursor to the CLP cell population stages, pointing to *Ostm1* as a positive modulator of the very early T cell program. The gl/gl thymus analysis demonstrates a major reduction of ETPs, an age-dependent marked swift and altered differentiation of DN subpopulations in the face of DP depletion and consequent decrease circulating T lymphoid cells. Targeted *Ostm1* expression initiating from early DN1 precursors to mature lymphocytes partially rescue the thymic reduction of gl/gl T cell subpopulations from the DN onward. This result with coculture analysis determines a cell-autonomous role for *Ostm1* in differentiation, independently of thymic epithelium. Characterization of the early DN1 T cell population transcriptome shows that *Ostm1* is a negative regulator of the *Foxo1-Klf2-S1pr1-Gnai1-Rac1* signaling axis implicated in thymic egression, intra-thymic T-cell DN differentiation, motility, and proliferation.

Importantly, major functions of *Ostm1* were identified through dysregulation of the gl/gl thymic ETP population and T cell successive differentiation stages within a temporal-dependent pattern. Before P8, our data demonstrate that *Ostm1* appears nonessential for the first fetal wave of gl/gl thymic precursor colonization and differentiation (Jotereau et al., 1987; Ramond et al., 2014). However, the altered architecture, decrease in size, in cellularity of DN, DP, and SP subpopulations of gl/gl thymus from P15, point to an essential temporal-dependent role of *Ostm1*. In fact this phenotype coincides with the second thymic precursor wave initiating at pre-neonatal ~E18 (Jotereau et al., 1987) and indicates that *Ostm1* is a major developmental regulator of the T-lymphoid program. Interestingly, the gl/gl T cell subpopulations, in accordance with *Ostm1* expression profile, vary throughout T cell successive differentiation stages. The substantial decrease of ~35-fold in the most immature gl/gl thymic ETP in parallel with robust *Ostm1* expression suggests that *Ostm1* plays a regulatory role in ETP cellular exponential increase, differentiation into T cell repertoire, and/or population maintenance. The reduced gl/gl ETP population and the relatively similar decrease in total DN population could be responsible in part for the striking temporal 100-fold depletion of the DP population. Alternatively, the mechanism leading to major decline of ETP and DN populations could be caused by high differentiation demand induced from the markedly low DP cell population. Nonetheless, *Ostm1* could also play a cell intrinsic role in DP with such an exceedingly low population in gl/gl thymus. Although the major deficit in total number of T lymphocytes in circulation can be a consequence of *Ostm1*'s impact on the early T cell differentiation program, one cannot rule out that *Ostm1* expression may also have a direct role in mature T cells. Such altered cellular differentiation profile can explain the gl/gl immunodeficiency and is compatible with the high susceptibility to infections of osteopetrotic ARO patients.

Characterization of ETP to DP differentiation in gl/gl delineates *Ostm1* as an important modulator of DN differentiation kinetic. The increased or similar proportion of DN1 cells in gl/gl at P15 or P21 in contrast to the marked decrease in DN2 and DN3 cell subpopulations highlights that *Ostm1* may control DN1 to DN2 transition phase as a checkpoint. The *ex vivo* rapid differentiation of DN cells from gl/gl ETP cocultured on notch-responsive stromal cell line is of strikingly similar magnitude to the *in vivo* thymic analysis. This similarity implies that *Ostm1* directly modulates the DN precursor differentiation rate independently of the thymic epithelium microenvironment. The *in vivo* accelerated DN differentiation kinetic in a temporal-dependent mode likely jeopardizes thymic cortical and medullary architecture as reported in the CD3ε26 transgenic mice (Hollander et al., 1995). In principle, a continual high rate of DN1-DN4 differentiation could impose a strong demand on the ETP cell population and yield a relatively higher proportion of DP cell subset as found *ex vivo*. On the contrary, DP population *in vivo* displays a further dramatic depletion suggesting an *Ostm1* function in DP, in addition to the regulatory role on DN differentiation.

This study demonstrates that *Ostm1* has *in vivo* cell-autonomous roles in distinct T cell differentiation stages. Although the CD2-*Ostm1* transgene does not seem to affect T cell differentiation profile *in vivo*, it virtually rescues gl/gl temporal-dependent T cell ontogeny from the DN1 subpopulation stage. This corrected phenotype
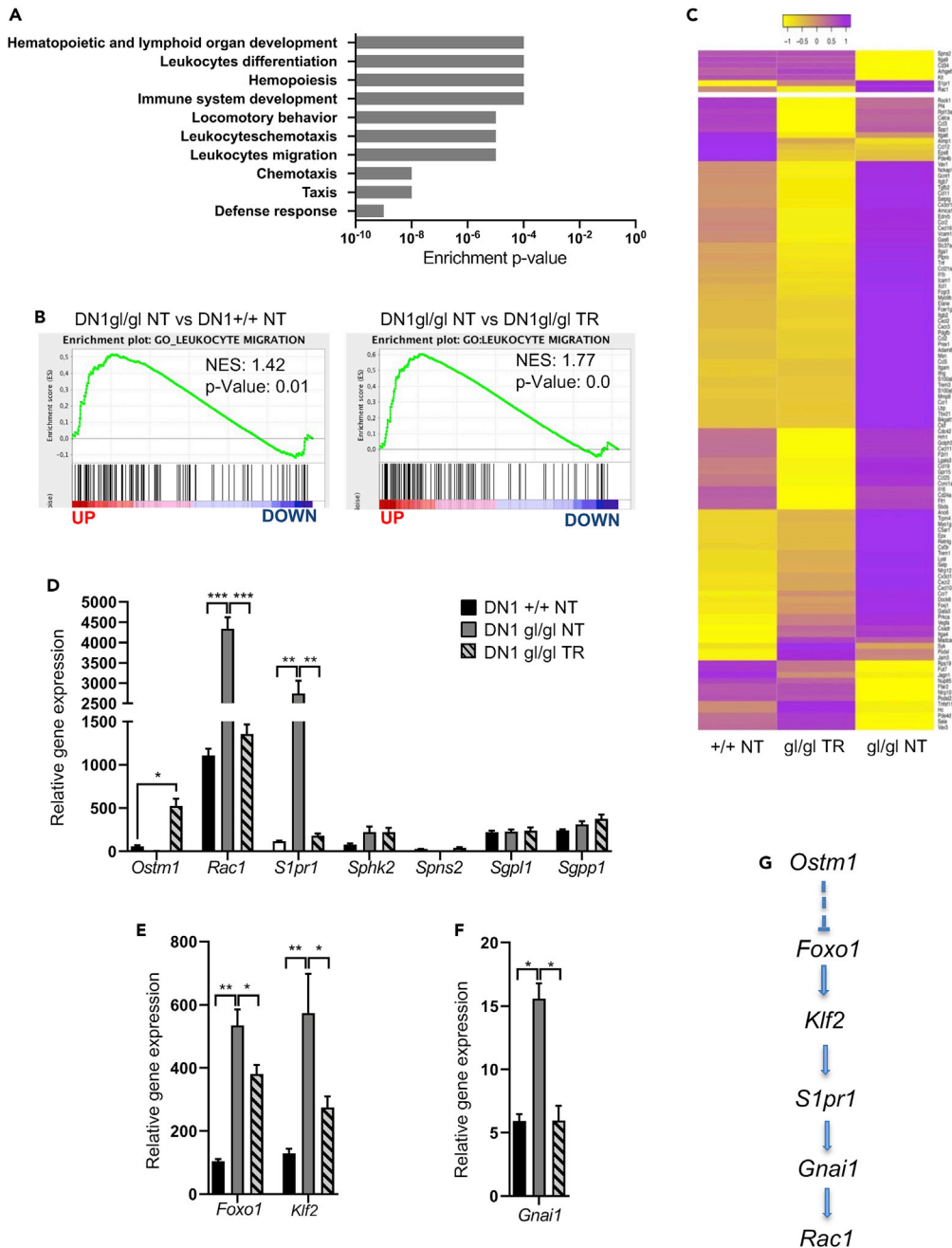
Figure 6. Loss of *Ostm1* in gl/gl DN1 T cell population crosstalk with a regulatory *S1pr1-Rac1* signaling axis

(A) Summary of Go terms and biological functions linked to differentially expressed genes across DN1 gl/gl NT in comparison to DN1 wild type (+/+ NT), with corresponding enrichment p values ranging from 10^{-9} to 10^{-4}.

(B) Gene Set Enrichment Score Analysis (GSEA) ranking migration-associated gene from top to bottom extreme, of upregulated or downregulated genes, within DN1 gl/gl NT sample was compared to DN1 wild type (+/+ NT) and gl/gl TR samples with normalized enrichment score (NES) and corresponding enrichment p values.

(C) Heat map of top differentially expressed migration-associated genes in DN1 gl/gl NT relative to DN1 wild type (+/+ NT) and gl/gl TR.

(D) Real time quantitative expression of *Ostm1*, *Rac1*, *S1pr1*, *Sphk2*, *Spns2*, *Sgpl1*, and *Sgpp1* genes in DN1 gl/gl NT relative to DN1 (+/+ NT) and DN1 gl/gl TR normalized to *S16* as internal control. Experiment was done in triplicate. *p < 0.05, **p < 0.01, ***p < 0.001. Data are represented as mean ± SEM.

Figure 6. *Continued*

(E) Real-time quantitative expression of *Foxo1* and *Klf2* genes within DN1 gl/gl NT in comparison to DN1 (+/+ NT) and DN1 gl/gl TR normalized to *S16* as internal control. Experiment was done in triplicate. *p < 0.05, **p < 0.01. Data are represented as mean ± SEM.

(F) Real time quantitative expression of *Gnai1* gene within DN1 gl/gl NT compared to DN1 (+/+ NT) and gl/gl TR normalized to *S16* as internal control. Experiment was done in triplicate. *p < 0.05. Data are represented as mean ± SEM.

(G) Schematic diagram showing the *Ostm1* signaling axis *Foxo1-Klf2-S1pr1-Gnai1-Rac1* identified in the present study as a critical pathway in the T cell lineage ontogeny and homeostasis.

provides compelling evidence that *Ostm1* predominantly acts in T cells and not in thymic epithelium corroborating *ex vivo* coculture results. The normalized kinetic and distribution of DN1-DN4, DP, and SP cells in CD2-*Ostm1* gl/gl transgenic shows that *Ostm1* is a regulator of T cell differentiation and population. The near rescue of thymus to body weight ratio correlates with improved thymic architecture in CD2-Ostm1 gl/gl transgenic mice. Importantly, the partially corrected number of CD2-*Ostm1* gl/gl thymic ETPs probably result from reduced pressure of the successive T cell differentiation stages. The remaining lower thymic ETP likely originates from cell-intrinsic function of *Ostm1* by modulating ETP survival, proliferation, and/or BM precursor differentiation. The comparable decrease in CD2-*Ostm1* gl/gl marrow CLPs and thymic ETPs suggests that *Ostm1* is not implicated in medullary egression or thymic homing. In fact, *Ostm1* in BM precursors may positively regulate the transition from the multipotent stem cells to the CLP stage. Further, the underdeveloped BM and defective osteoclasts in CD2-*Ostm1* gl/gl mice show that *Ostm1* does not play a role in the well-known T-cell crosstalk with osteoclast (Takayanagi, 2007) but carries cell-autonomous function in these lineages. Altogether, *Ostm1* plays a temporal-dependent role in distinct and critical stages of T cell ontogeny, from CLP to ETP, DN, and DP.

Another key finding from this study is the *Ostm1* molecular mechanism(s) in thymic T cell differentiation program. From transcriptome signatures of sorted DN1 gl/gl, normalized in CD2-*Ostm1* gl/gl, we uncovered a crosstalk between *Ostm1* and *Foxo1-Klf2-S1pr1-Gnai1-Rac1* signaling axis. Significantly, *Ostm1* ablation led to enhanced *Foxo1* expression in the early DN1 cell subpopulation, both with functional roles in osteoclast progenitors via NFATc1 (Pata and Vacher, 2018; Tan et al., 2015; Wang et al., 2015). Interestingly, *Foxo1* is a direct transcriptional regulator of *Klf2* (Kerdiles et al., 2009) that is also upregulated in gl/gl DN1. Though *Klf2* regulates T cell trafficking, quiescence, and survival (Carlson et al., 2006), overexpression of *Klf2* was shown to promote cell-cycle withdrawal by repressing c-Myc transcription and/or inducing p21$^{WAF1/CIP1}$ (Buckley et al., 2001; Wu and Lingrel, 2004). Hence *Ostm1* may indirectly be a positive regulator of cell proliferation, trafficking, or survival. The specific upregulation of the GPCR S1P$_1$, a transcriptional target of *Klf2*, in DN1 cells independently of S1P family members *infers* a cell intrinsic mechanism. This intrinsic mechanism for *S1pr1* is also supported by other GPCR that become constitutively active upon overexpression (Burstein et al., 1995; Lee et al., 1996; Milano et al., 1994). Consistent with gl/gl phenotype, inducible transgenic *S1pr1* mice show altered DN profile with reduced DN2 to DN4 cell subpopulations (Blaho et al., 2015). Such DN decrease associated with altered kinetic of differentiation in gl/gl likely results in disrupted thymic architecture from atypical transitions of cell differentiation stages and cortical migration, two phenomena intertwined in thymus morphologic structure (Bhandoola et al., 2007; Porritt et al., 2003). The upregulation of *S1pr1* in gl/gl could affect thymic cellularity by modulating DN1 cell subset, and possibly, additional T-cell subpopulations. Because *S1pr1* plays a well-known role in T-cell egression and migration (Allende et al., 2004; Golan et al., 2012; Matloubian et al., 2004; Thangada et al., 2010), it may promote gl/gl T cell DN1 subpopulation egression from the thymus, although the DN1 levels are not proportionally decreased. Importantly, *S1pr1* overexpression in transgenic mice was shown, like for *Klf2*, to have reduced T cell proliferation rate that may prevail in gl/gl (Blaho et al., 2015; Dorsam et al., 2003; Gräler et al., 2005). S1P$_1$ transmits signals by coupling exclusively to the Gα$_i$ (Lee et al., 1996; Rivera et al., 2008). Of interest, *Gnai1*, induced in gl/gl, has been implicated in DN1-DN2 transition, T cell trafficking, and thymus cellularity (Hwang et al., 2017). Among the specific signaling effectors regulated by S1P$_1$-Gαi interaction is the small G protein Rac1 (Ishii et al., 2010; Sanchez and Hla, 2004; Takuwa, 2002) strongly overexpressed in gl/gl. Activation of Rac1 via S1P$_1$-Gα$_i$, likely regulates the rate of gl/gl DN differentiation kinetic and cell motility. This mechanism is supported by accelerated DN transition stages in constitutively active Rac1 transgenic T cells, possibly by modulating actin polymerization dynamics and cell motility (Gomez et al., 2000, 2001). Similar cellular processes have also been characterized for *Ostm1* and *S1pr1* in osteoclast cystoskeletal rearrangement, motility, and chemotaxis (Ishii et al., 2009; Rajapurohitam et al., 2001). Further, the parallel between *Rac1* and *Ostm1* also extends to the DN CD25 intermediate cell population because the active *Rac1* transgenic causes downregulation of CD25 in T cell precursors (Gomez et al., 2000, 2001). In fact, the reduced CD25 or IL2R promoting proliferation could also contribute to the gl/gl DN-cell differentiation pattern, thymus low cellularity, and abnormal architecture.

Given that ablation of *Ostm1* can enhance expression of *S1pr1* in DN1 cells, one could reason that *Ostm1* modulates *S1pr1* at an earlier stage of T cell ontogeny, specifically in marrow CLP and thymic ETP cell populations. A previous study has shown that overexpression of *S1pr1* in multipotent hematopoietic cells suppressed CLP and ETP via limited proliferation (Blaho et al., 2015). Consistently, restrained BM lymphopoiesis in gl/gl and gl/gl TR early T cell ontogeny may result from $S1P_1$ induction in hematopoietic multipotent to CLP transition. Moreover, the strikingly reduced DP population in the absence of *Ostm1* may also be attributed to *S1pr1* signaling. Indeed, transgenic overexpression of *S1pr1* results in a major decrease in the DP cell population (Blaho et al., 2015; Gomez et al., 2001). We cannot exclude either that an enhanced expression of *S1pr1* could also play a role in T cell egression and migration in the gl/gl phenotype. Most importantly, activation of *Foxo1-Klf2-S1pr1-Gnai1-Rac1* signaling axis detected upon *Ostm1* depletion elucidates most of the gl/gl T lymphopoietic phenotype.

In summary *Ostm1* is essential for regulation of the medullary T cell precursors to lymphocyte cell populations in a temporal-dependent pattern and for the distinct CLP, ETP, DN, and DP stages. Importantly, the *Ostm1* cellular mechanism demonstrates a cell-autonomous role on the rate and maintenance of thymic T-cell differentiation. Our study also defines a predominant crosstalk of *Ostm1* with the *Foxo1-Klf2-S1pr1-Gnai1-Rac1* signaling pathway that is central in T lymphopoiesis and homeostasis.

Limitations of this study

Our *Ostm1* expression studies in different T cell progenitor stages were focused on transcriptional analyses, as endogenous Ostm1 protein cannot be detected with the antibodies generated by us and others. Our transcriptome study identified not only an *Ostm1* crosstalk with *Foxo1*, *Klf2*, *S1pr1*, *Gnai1*, and *Rac1*. We also uncovered a new activated signaling pathway *Foxo1-Klf2-S1pr1-Gnai1-Rac1* axis in *Ostm1* null DN cells that could be further supported via genetic inhibition of one of the upstream effectors.

STAR★METHODS

Detailed methods are provided in the online version of this paper and include the following:

- KEY RESOURCES TABLE
- RESOURCE AVAILABILITY
  - Lead contact
  - Materials availability
  - Data and code availability
- EXPERIMENTAL MODEL AND SUBJECT DETAILS
- METHOD DETAILS
  - Generation of transgenic animals
  - Gene and protein expression
  - Flow cytometry analysis and cell sorting
  - Histological and X-ray analysis
  - Hematologic parameters
  - Cell cultures
  - RNA sequencing
  - Computational analysis
- QUANTIFICATION AND STATISTICAL ANALYSIS

SUPPLEMENTAL INFORMATION

Supplemental information can be found online at https://doi.org/10.1016/j.isci.2022.104160.

AUTHOR CONTRIBUTIONS

M.M. and J.V. conceived the project. M.M. and M.P. carried out the experiments and assessed the data with supervision and analysis from J.V. M.M. assembled an initial draft and J.V. wrote the manuscript.

DECLARATION OF INTERESTS

The authors declare no competing interests.

REFERENCES

Allende, M.L., Dreier, J.L., Mandala, S., and Proia, R.L. (2004). Expression of the sphingosine 1-phosphate receptor, S1P1, on T-cells controls thymic emigration. J. Biol. Chem. 279, 15396–15401.

Bai, A., Hu, H., Yeung, M., and Chen, J. (2007). Kruppel-like factor 2 controls T cell trafficking by activating L-selectin (CD162L) and sphingosine-1-phospahte receptor 1 transcription. J. Immunol. 178, 7632–7639.

Bhandoola, A., von Boehmer, H., Petrie, H.T., and Zúñiga-Pflücker, J.C. (2007). Commitment and developmental potential of extrathymic and intrathymic T cell precursors: plenty to choose from. Immunity 26, 678–689.

Blaho, V.A., Galvani, S., Engelbrecht, E., Liu, C., Swendeman, S.L., Kono, M., RProia, R.L., Steinman, L., Han, M.H., and Hla, T. (2015). HDL-bound sphingosine-1-phosphate restrains lymphopoiesis and neuroinflammation. Nature 523, 342–346.

Bleul, C.C., Corbeaux, T., Reuter, A., Fisch, P., Mönting, J.S., and Boehm, T. (2006). Formation of a functional thymus initiated by a postnatal epithelial progenitor cell. Nature 441, 992–996.

Blin-Wakkach, C., Wacchach, A., Sexton, P.M., Rochet, N., and Carle, G.F. (2004). Hematological defects in oc/oc mouse, a model of infantile malignant osteopetrosis. Leukemia 18, 1505–1511.

Brodeur, J.-F., Li, S., da Silva Martins, M., Larose, L., and Dave, V.P. (2009). Critical and multiple roles for the CD3 e intracytoplasmic tail in double negative to double positive thymocyte differentiation. J. Immunol. 182, 4844–4853.

Buckley, A.F., Kuo, C.T., and Leiden, J.M. (2001). Transcription factor LKLF is sufficient to program T cell quiescence via a c-Myc-dependent pathway. Nat. Immunol. 2, 698–704.

Burstein, E.S., Spalding, T.A., Brauner-Osborne, H., and Brann, M.R. (1995). Constituttive activation of muscarinic receptors by the G-protein Gq. FEBS Lett. 363, 261–263.

Carlson, C.M., Endrizzi, B.T., Wu, J., Ding, X., Weinreich, M.A., Walsh, E.R., Wani, M.A., Lingrel, J.B., Hogquist, K.A., and Jameson, S.C. (2006). Kruppel-like factor 2 regulates thymocyte and T-cell migration. Nature 442, 299–302.

Chalhoub, N., Benachenhou, N., Rajapurohitam, V., Pata, M., Ferron, M., Frattini, A., Villa, A., and Vacher, J. (2003). Grey-lethal mutation induces severe malignant autosomal recessive osteopetrosis in mouse and human. Nat. Med. 9, 399–406.

Cyster, J.G. (2009). Settling the thymus: immigration requirements. J. Exp. Med. 206, 731–734.

de Boer, J., Williams, A., Skavdis, G., Harker, N., Coles, M., Tolaini, M., Norton, T., Williams, K., Roderick, K., Potocnik, A.J., et al. (2003). Transgenic mice with hematopoietic and lymphoid specific expression of Cre. Eur. J. Immunol. 33, 314–325.

Dorsam, G., Graeler, M.H., Seroogy, C., Kong, Y., Voice, J.K., and Goetzl, E.J. (2003). Transduction of multiple effects of sphingosine 1-phosphate (S1P) on T cell functions by the S1P1 G protein-coupled receptor. J. Immunol. 171, 3500–3507.

Ferron, M., Boudiffa, M., Arsenault, M., Rached, M., Pata, M., Giroux, S., Elfassihi, L., Kisseleva, M.V., Majerus, P.W., Rousseau, F., et al. (2011). Inositol Polyphosphate 4-phosphatase b as a regulator of bone mass in mice and humans. Cell Metab. 14, 466–477.

Frattini, A., Orchard, P.J., Sobacchi, C., Giliani, S., Abinun, M., Mattsson, J.P., Keeling, D.J., Andersson, A.-K., Wallbrandt, P., Zecca, L., et al. (2000). Defects in TCIRG1 subunit of the vacuolar proton pump are responsible for a subset of human autosomal recessive osteopetrosis. Nat. Genet. 25, 343–346.

Golan, K., Vagima, Y., Ludin, A., Itkin, T., Cohen-Gur, S., Kalinkovich, A., Kollet, O., Kim, C., Schajnoviz, A., Ovadya, Y., et al. (2012). S1P promotes murine progenitor egress and mobilization via S1P1-mediated ROS signaling and SDF-1 release. Blood 119, 2478–2488.

Gomez, M., Tybulewicz, V.L.J., and Cantrell, D.A. (2000). Control of pre-T cell proliferation and differentiation by the GTPase Rac-1. Nat. Immunol. 1, 348–352.

Gomez, M., Kioussis, D., and Cantrell, D.A. (2001). The GTPase rac-1 controls cell fate in the thymus by diverting thymocytes from positive to negative selection. Immunity 15, 700–713.

Gossens, K., Naus, S., Corbel, S.Y., Lin, S., Rossi, F.M., Kast, J., and Ziltener, H.J. (2009). Thymic progenitor homing and lymphocyte homeostasis are linked via S1P-controlled expression of thymic P-selectin/CCL25. J. Exp. Med. 206, 761–778.

Gräler, M.H., Huang, M.C., Watson, S., and Goetzl, E.J. (2005). Immunological effects of transgenic constitutive expression of the type 1 sphingosine 1-phosphate receptor by mouse lymphocytes. J. Immunol. 174, 1997–2003.

Guerrini, M.M., Sobacchi, C., Cassani, B., Abinun, M., Kilic, S.S., Pangrazio, A., Moratto, D., Mazzolari, E., Clayton-Smith, J., Orchard, P., et al. (2008). Human osteoclast-poor osteopetrosis with hypogammaglobulinemia due to TNFRSF11A (RANK) mutations. Hum. Mol. Genet. 83, 64–76.

Héraud, C., Griffiths, A., Pandruvada, S.N.M., Kilimann, M.W., Pata, M., and Vacher, J. (2014). Severe neurodegeneration with impaired autophagy mechanism triggered by Ostm1 deficiency. J. Biol. Chem. 289, 13912–13925.

Hollander, G.A., Wang, B., Nichoglannopoulou, A., Platenburg, P.P., van Ewijk, W., Burakoff, S.J., Guttirez-Ramos, J.-C., and Terhorst, C. (1995). Developmental control point in induction of thymic cortex regulated by a subpopulation of prothymocytes. Nature 373, 350–353.

Hwang, I.-Y., Harrison, K., Park, C., and Kehrl, J.H. (2017). Loss of Gai proteins impairs thymocyte development, disrupts T-cell trafficking, and leads to an expanded population of splenic CD4+PD-1+CXCR5+/- T-cells. Sci. Rep. 7, 4156.

Ishii, M., Egen, J.G., Klauschen, F., Meir-Schellersheim, M., Saeki, Y., Vacher, J., Proia, R.L., and Germain, R.N. (2009). Sphingosine-1-phosphate mobilizes osteoclast precursors and regulates bone homeostasis. Nature 458, 524–528.

Ishii, M., Kikuta, J., Shimazu, Y., Meir-Schllersheim, M., and Germain, R.N. (2010). Chemorepulsion by blood S1P regulates osteoclast precursor mobilization and bone remodeling in vivo. J. Exp. Med. 207, 2793–2798.

Jotereau, F.V., Heuze, F., Salomon-Vie, V., and Gascan, H. (1987). Cell kinetics in the fetal mouse thymus: precursor cell input, proliferation and emigration. J. Immunol. 138, 1026–1030.

Kerdiles, Y.M., Beisner, D.R., Tinoco, R., Dejean, A.S., Castrillon, D.H., DePinho, R.A., and Hedrick, S.M. (2009). Foxo1 links homing and survival of naive T cells by regulating L-selectin, CCR7 and interleukin 7 receptor. Nat. Immunol. 10, 176–184.

Kollet, O., Dar, A., Shivtiel, S., Kalinkovich, A., Lapid, K., Sztainberg, Y., Tesio, M., Samstein, R.M., Goichberg, P., Spiegel, A., et al. (2006). Osteoclasts degrade endosteal components and

promote mobilization of hematopoietic progenitor cells. Nat. Med. 12, 657–664.

Kornak, U., Kasper, D., Bösl, M.R., Kaiser, E., Schweizer, M., Schulz, A., Friedrich, W., Delling, G., and Jentsch, T.J. (2001). Loss of the ClC-7 chloride channel leads to osteopetrosis in mice and man. Cell 104, 205–215.

Lee, M.-J., Evans, M., and Hla, T. (1996). The inducible G protein-coupled receptor edg-1 signals via the Gi/mitogen-activated protein kinase pathway. J. Biol. Chem. 271, 11271–11279.

Lymperi, S., Ersek, A., Ferraro, F., Dazzi, F., and Horwood, N.J. (2011). Inhibition of osteoclast function reduces hematopoietic stem cell numbers in vivo. Blood 117, 1540–1549.

Mansour, A., Abou-Ezzi, G., Sitnicka, E., Jacobsen, S.E., Wakkach, A., and Blin-Wakkach, C. (2012). Osteoclasts promote the formation of hematopoietic stem cell niches in the bone marrow. J. Exp. Med. 209, 537–549.

Maranda, B., Chabot, G., Décarie, J.-C., Pata, M., Azeddine, B., Moreau, A., and Vacher, J. (2008). Clinical and cellular manifestations of OSTM1 related infantile osteopetrosis. J. Bone Miner. Res. 23, 296–300.

Matloubian, M., Lo, C.G., Cinamom, G., Lesneski, M.J., Xu, Y., Brinkmann, V., Allende, M.L., Proia, R.L., and Cyster, J.G. (2004). Lymphocyte egress from thymus and peripheral lymphoid organs is dependent on S1P receptor 1. Nature 427, 355–360.

Mazzolari, E., Forino, C., Razza, A., Porta, F., Villa, A., and Notarangelo, L.D. (2009). A single-center experience in 20 patients with infantile malignant osteopetrosis. Am. J. Hematol. 84, 473–479.

Milano, C.A., Dolber, P.C., Rockman, H.A., Bond, R.A., Venable, M.E., Allen, L.F., and Lefkowitz, R.J. (1994). Myocardila expression of a constitutive active alpha1B-adrenergic receptor in transgenic mice induces cardiac hypertrophy. Proc. Natl. Acad. Sci. U S A 91, 10109–10113.

Misslitz, A., Pabst, O., Hintzen, G., Ohl, L., Kremmer, E., Petrie, H.T., and Forster, R. (2004). Thymic T cell development and progenitor localization depend on CCR7. J. Exp. Med. 200, 481–491.

Mohtashami, M., Shah, D.K., Kianizad, K., Awong, G., and Zúñiga-Pflücker, J.C. (2013). Induction of T-cell development by Delta-like 4-expressing fibroblasts. Int. Immunol. 25, 601–611.

Mohtashami, M., and Zúñiga-Pflucker, J.C. (2006). Three-dimensional architecture of the thymus is required to maintain delta-like expression necessary for inducing T cell development. J. Immunol. 176, 730–734.

Orchard, P.J., Fasth, A.L., Le Radmacher, J., He, W., Boelens, J.J., Horwitz, E.M., Al-Seraihy, A., Ayas, M., Binfim, C.M., Boulad, F., et al. (2015). Hematopoietic stem cell transplantation for infantile osteopetrosis. Blood 126, 270–276.

Ott, C.E., Fischer, B., Schröter, P., Richter, R., Gupta, N., Verma, N., Kabra, M., Mundlos, S., Rajab, A., Neitzel, H., et al. (2013). Severe neuronopathic autosomal recessive osteopetrosis due to homozygous deletions affecting OSTM1. Bone 55, 292–297.

Pandruvada, S.N., Beauregard, J., Benjannet, S., Pata, M., Lazure, C., Seidah, N.G., and Vacher, J. (2016). Role of Ostm1 cytosolic complex with kinesin 5B in intracellular dispersion and trafficking. Mol. Cell. Biol. 36, 507–521.

Pangrazio, A., Cassani, B., Guerrini, M.M., Crockett, J.C., Marella, V., Zammataro, L., Strina, D., Schulz, A., Schlack, C., Kornak, U., et al. (2012). RANK-dependent autosomal recessive osteopetrosis: characterization of five new cases with novel mutations. J. Bone Miner. Res. 27, 342–351.

Pata, M., and Vacher, J. (2018). Ostm1 bifunctional roles in osteoclast maturation: insights from a mouse model mimicking a human OSTM1 mutation. J. Bone Miner. Res. 33, 888–898.

Pata, M., Héraud, C., and Vacher, J. (2008). OSTM1 bone defect reveals an intercellular hematopoietic crosstalk. J. Biol. Chem. 283, 30522–30530.

Porritt, H.E., Gordon, K., and Petrie, H.T. (2003). Kinetics of steady-state differentiation and mapping of intrathymic-signaling environments by stem cell transplantation in nonirradiated mice. J. Exp. Med. 198, 957–962.

Quarello, P., Forni, M., Barbereis, L., Defilippi, C., Campagnoli, M.F., Frattini, A., Chalhoub, N., Vacher, J., and Ramenghi, U. (2004). Severe malignant osteopetrosis due to a Gl gene mutation. J. Bone Miner. Res. 19, 1194–1199.

Rajapurohitam, V., Chalhoub, N., Benachenhou, N., Neff, L., Baron, R., and Vacher, J. (2001). The mouse osteopetrotic grey-lethal mutation induces a defect in osteoclast maturation/function. Bone 28, 513–523.

Ramond, C., Berthault, C., Burlen-Dfranoux, O., de Sousa, A.P., Guy-Grand, D., Vieira, P., and Cumnao, A. (2014). Two waves of disctinct hematopoeitic cells colonize the fetal thymus. Nat. Immunol. 15, 27–35.

Reeves, J.D., August, C.S., Humbert, J.R., and Weston, W.L. (1979). Host defense in infantile osteopetrosis. Pediatrics 64, 202–206.

Rivera, J., Proia, R.L., and Olivera, A. (2008). The alliance of sphingosine-1-phosphate and its receptors in immunity. Nat. Rev. Immunol. 8, 753–763.

Sanchez, T., and Hla, T. (2004). Structural and functional charactistics of S1P receptors. J. Cell. Biochem. 92, 913–922.

Scimeca, J.-C., Franchi, A., Trojani, C., Parrinello, H., Grosgeorge, J., Robert, C., Jaillon, O., Poirier, C., Gaudray, P., and Carle, G.F. (2000). The gene encoding the mouse homologue of the human osteoclast-specific 116-kDa V-ATPase subunit bears a deletion in osteosclerotic (oc/oc) mutants. Bone 26, 207–213.

Shah, D.K., and Zúñiga-Pflucker, J.C. (2014). An overview of the intrthymic intricacies of T cell development. J. Immunol. 192, 4017–4023.

Sobacchi, C., Schulz, A., Coxon, F.P., Villa, A., and Helfrich, M.H. (2013). Osteopetrosis: genetics, treatment and new insights into osteoclast function. Nat. Rev. Endocrinol. 9, 522–536.

Takayanagi, H. (2007). Osteoimmunology: shared mechanisms and crosstalk between the immune and bone systems. Nat. Rev. Immunol. 7, 292–304.

Takayanagi, H., Ogasawara, K., Hida, S., Chiba, T., Murata, S., Sato, K., Takaota, A., Yokochi, T., Oda, H., Tanaka, K., et al. (2000). T-cell mediated regulation of osteoclastogenesis by signalling cross-talk between RANKL and IFN-g. Nature 408, 600–605.

Takuwa, Y. (2002). Subtype-specific differential regulation of Rho family G proteins and cell migration by the Edg family sphingosine-1-phosphate receptors. Biochem. Biophys. Acta 1582, 112–120.

Tan, P., Guan, H., Xie, L., Mi, B., Fang, Z., Li, J., and Li, F. (2015). FOXO1 inhibits osteoclastogenesis partially by antagnozing MYC. Sci. Rep. 5, 16835.

Thangada, S., Khanna, K.M., Blaho, V.A., Oo, M.L., Im, D.-S., Guo, C., Lefrancois, L., and Hla, T. (2010). Cell-surface residence of sphingosine 1-phosphate receptor 1 on lymphocytes determines lymphocyte egress kinetics. J. Exp. Med. 207, 1475–1483.

Trapnell, C., Roberts, A., Goff, L., Pertea, G., Kim, D., Kelley, D.R., Pimentel, H., Salzberg, S.L., Rinn, J.L., and Pachter, L. (2012). Differential gene and transcript expression analysis of RNA-seq experiments with TopHat and Cufflinks. Nat. Protoc. 7, 562–578.

Wang, Y., Dong, G., Jeon, H.H., Elazizi, M., La, L.B., Hameedaldeen, A., Xiao, E., Tian, C., Alsadun, S., Choi, Y., et al. (2015). FOXO1 mediates RANKL-induced osteoclast formation and activity. J. Immunol. 194, 2878–2887.

Weinreich, M.A., and Hogquist, K.A. (2008). Thymic emigration: when and how T cells leave home. J. Immunol. 181, 2265–2270.

Wu, J., and Lingrel, J.B. (2004). KLF2 inhibits jurkat T leukemia cell growth via upregulation of cyclin-dependent kinase inhibitor p21 WAF!/CIP1. Oncogene 23, 8088–8096.

Xiao, L., Zhou, Y., Frils, T., Beagley, K., and Xiao, Y. (2019). S1P-S1PR1 signaling: the "Sphinx" in osteoimmunology. Front. Immunol. 10, 1409.

Yokota, T. (2006). Tracing the first waves of lymphopoiesis in mice. Development 133, 2041–2051.

Zhumabekov, T., Corbella, P., Tolaini, M., and Kioussis, D. (1995). Improved version of a human CD2 minigene based vector for T cell-specific expression in transgenic mice. J. Immunol. Methods 185, 133–140.

Zúñiga-Pflucker, J.C. (2009). The original intrathymic progenitor from which T cells originate. J. Immunol. 183, 3–4.

STAR★METHODS

KEY RESOURCES TABLE

REAGENT or RESOURCE	SOURCE	IDENTIFIER
Antibodies		
Mouse monoclonal Anti-β-Actin Antibody	Sigma-Aldrich	Cat# A5441, RRID:AB_476744
Mouse monoclonal Anti-V5-HRP	Invitrogen	Cat# R961-25, RRID: AB_2556565
Goat anti-mouse IgG HRP Conjugated	Bio-Rad	Cat# 1706516
CD4 Monoclonal Antibody (GK1.5) - PE conjugated	eBioscience	Cat# 12-0041-82, RRID: AB_465506
TCR beta Monoclonal Antibody (H57-597) - PE conjugated	eBioscience	Cat# 12-5961-82, RRID: AB_466066
CD8a Monoclonal Antibody (53-6.7) – FITC conjugated	eBioscience	Cat# 11-0081-82, RRID: AB_464915
CD44 Monoclonal Antibody (IM7) - FITC conjugated	eBioscience	Cat# 11-0441-82, RRID: AB_465045
CD62P (P-Selectin) Monoclonal Antibody (Psel.KO2.3) – APC conjugated	eBioscience	Cat# 17-0626-82, RRID: AB_11217675
CD117 (c-Kit) Monoclonal Antibody (ACK2)– APC conjugated	eBioscience	Cat# 17-1172-82, RRID: AB_469433
CD69 Monoclonal Antibody (H1.2F3) – APC conjugated	eBioscience	Cat# 17-0691-82, RRID: AB_1210795
CD25 Monoclonal Antibody (PC61.5) - PE-Cyanine7 conjugated	eBioscience	Cat# 25-0251-82, RRID: AB_469608
Ly-6A/E (Sca-1) Monoclonal Antibody (D7) - PE-Cyanine7 conjugated	eBioscience	Cat# 25-5981-82, RRID: AB_469669
Mouse Hematopoietic Lineage Biotin Panel (Ter119, CD3e, CD11b, B220, Gr1)	eBioscience	Cat# 88-7774, RRID: AB_476399
CD4 Monoclonal Antibody (GK1.5) - Biotin conjugated	eBioscience	Cat# 13-0041-82, RRID: AB_466325
CD8 Monoclonal Antibody (53-6.7) - Biotin conjugated	BD Pharmigen	Cat# 553029, RRID: AB_394567
CD49Monoclonal Antibody (DX5) - Biotin conjugated	BD Pharmigen	Cat# 553856, RRID: AB_395092
TCRγδ Monoclonal Antibody (GL-3) - Biotin conjugated	eBioscience	Cat# 13-5711-82, RRID: AB_466668
NK1.1 Monoclonal Antibody (PK136) - Biotin conjugated	eBioscience	Cat# 13-5941-82, RRID: AB_466804
CD5 Monoclonal Antibody (53-7.3) - Biotin conjugated	eBioscience	Cat# 13-0051-81, RRID: AB_466338
IgM Monoclonal Antibody (II/41) - Biotin conjugated	eBioscience	Cat# 13-5790-81, RRID: AB_466674
IL7R Monoclonal Antibody (A7R34) - Biotin conjugated	eBioscience	Cat# 13-1271-81, RRID: AB_466587
Streptavidin – FITC conjugated	BD Pharmigen	Cat# 554060, RRID: AB_10053373
Chemicals, peptides, and recombinant proteins		
Trizol	Life technologies	Cat# 15596026
M-MuLV Reverse Transcriptase	NEB	Cat# M0253S
MagMAX™ Total Nucleic Acid Isolation Kit	Life technologies	Cat# AM1840
qScript cDNA supermix Quanta	VWR	Cat# 101414-102
SYBR Green Master Mix	Qiagen	Cat# 203443
Bionanalyzer RNA pico chips	Agilent	Cat# 5067-1513
Recombinant Murine Flt3-Ligand	PeproTech	Cat# 250-31L
Recombinant Murine SCF	PeproTech	Cat# 250-03
Recombinant Murine IL-7	PeproTech	Cat# 217-17
Deposited data		
The RNA seq data	N/A	GSE72184
Experimental models: Cell lines		
OP9 Bone stromal cells	ATCC	Cat# CRL-2749, RRID:CVCL_4398
Experimental models: Organisms/strains		
Mouse GL/Le dl^J +/+ gl	The Jackson Laboratory	Cat# JAX:000255; RRID: IMSR_JAX:000255

Continued

REAGENT or RESOURCE	SOURCE	IDENTIFIER
Oligonucleotides		
Table S4 for Genotyping primers	Invitrogen	N/A
Table S5 for qPCR primers	Invitrogen	N/A
Software and algorithms		
FlowJo v10.4	BD	https://www.flowjo.com/solutions/flowjo; RRID: SCR_008520
Fiji-ImageJ	National Institute of Health	https://imagej.net/Fij; RRID: SCR_003070
GraphPad Prism 10	GraphPad	https://www.graphpad.com/scientific-software/prism/; RRID: SCR_002798
Image Lab Software	Bio-Rad	http://www.bio-rad.com/en-us/sku/1709690-image-lab-software; RRID: SCR_014210
Cuffdiff 2.2.1	N/A	http://cole-trapnell-lab.github.io/cufflinks/install
CummeRbund 2.6.1	N/A	http://compbio.mit.edu/cummeRbund
R 3.1.0	N/A	https://cran.r-project.org/bin/windows/base/old/3.1.0
Ingenuity Pathway Analysis (IPA)	N/A	https://digitalinsights.qiagen.com/products-overview/discovery-insights-portfolio/analysis-and-visualization/qiagen-ipa
Annotation Visualization and Integrated Discovery (DAVID)	N/A	https://david.ncifcrf.gov
Gene Set Enrichment Analysis (GSEA)	N/A	http://software.broadinstitute.org/gsea/index.jsp

RESOURCE AVAILABILITY

Lead contact

Further information and requests for resources and reagents should be directed to and will be fulfilled by the lead contact, Jean Vacher (vacherj@ircm.qc.ca).

Materials availability

Plasmids generated in his study are available upon request from the lead contact, Jean Vacher (vacherj@ircm.qc.ca).

Data and code availability

Data reported in this paper will be shared by the lead contact upon request. The RNA-seq data reported herein have been deposited in the Gene Expression Omnibus (GEO) database under accession number GSE72184. This paper does not report original code. Any additional information required to reanalyze the data reported in this paper is available from the lead contact upon request

EXPERIMENTAL MODEL AND SUBJECT DETAILS

The mouse strain GL/Le dl^J +/+ gl was obtained from The Jackson Laboratory (Bar Harbor, ME) and maintained by heterozygous brother x sister mating for ~200 generations. Mice were housed under pathogen-free conditions (12/12-h dark/light cycles, 22°C, and 50% humidity) and fed with Irradiated Global 18% Protein Rodent Diet, Code 2918, Envigo, Teklad, Madison, WI. All experiments were performed on 3-week-old males and females mice and littermates served as controls. Animal protocols complied with the guidelines of the Canadian Committee for Animal protection and were approved by the local IRCM institutional animal care committee.

METHOD DETAILS

Generation of transgenic animals

CD2-*Ostm1* transgene was produced by introduction of the V5-*Ostm1* tagged cDNA (1.055 kb) downstream of the human CD2 promoter (−5200/+1) and upstream of poly (A) signal and hCD2 locus control region (LCR, 6 kb) (Zhumabekov et al., 1995). The linear CD2-*Ostm1* fragment (Sal1-Not1) was injected to generate transgenic mice (Héraud et al., 2014; Pata et al., 2008) and founders were identified by PCR. Primer sequences used are listed in the key resources table (Table S4). PCR amplification conditions were 94°C, 5 min, followed by 30 cycles of 94°C for 30 s, 65°C for 30 s, and 72°C for 10 min. Heterozygous gl/+ mice were identified (Chalhoub et al., 2003) and were mated to transgenic CD2-*Ostm1* lines to generate gl/gl CD2-*Ostm1* (gl/gl TR).

Gene and protein expression

Total RNA was isolated from murine tissues (bone marrow, brain, kidney, thymus, liver, spleen) with Trizol (Invitrogen). Total RNA from sorted thymocytes was isolated using MagMax kit (Life technologies). RNA (50 ng–300 ng) was used for cDNA synthesis using qScript cDNA supermix (Quanta biosciences). Gene expression was assessed in triplicates by quantitative real-time PCR (qPCR) with SYBR Green Master Mix (Qiagen). Primer sequences used are listed in the key resources table (Table S5). PCR conditions were 94°C, 15 min, followed by 50 cycles of 94°C for 0.5 min, 55°C for 0.5 min, and 72°C for 0.5 min in an MX4000 Mutiplex quantitative PCR analyzer. For primer sequences used, see key resources table.

Proteins were isolated from hematopoietic tissues and brain in RIPA buffer (Ferron et al., 2011). Western blots were probed with anti-V5-HRP (Invitrogen; 1:5000) and β-actin (Sigma) antibodies in TBST1X supplemented with 3% BSA overnight at 4°C, washed 3 times in TBST and incubated 1 h with anti-mouse IgG HRP (1:10000) (Bio-Rad). Signals were revealed by the ECL detection system (Amersham Biosciences) and image was visualized and quantified with Bio-Rad Image lab software.

Flow cytometry analysis and cell sorting

Flow cytometry analysis (FACS) was carried out on spleen, thymus, bone marrow and lymph node single cell suspension in phosphate-buffered saline supplemented with 1% heat-inactivated fetal bovine serum. Nucleated cells (1.5 × 10^6) were stained with the following antibodies: phycoerythrin-conjugated (PE) anti-CD4, anti-TCR-β, Streptavidin; fluorescein isothiocyanate-conjugated (FITC) anti-CD8, anti-CD44, anti-Streptavidin; APC conjugated anti-CD62, anti-cKit, anti-CD44, anti-CD69; Phycoerythrin (pe)-Cy7 conjugated anti-CD25, anti-Sca1; biotin conjugated lineage cocktail (Ter119, CD4, CD8, DLX5, B220, Gr1, CD11b, CD3e, TCRγδ, NK1.1, CD5, IgM and IL7R). Data acquisition and analysis were respectively done with CellQuest and FlowJo software on a BD FACS Calibur four-color flow cytometer and BD LSR cytometer. Cell sorting was performed on Moflo cytometer.

Histological and X-ray analysis

Thymi from P8, P15 and P21 mice were fixed in 10% phosphate-buffered formalin and embedded in paraffin. Tissue sections were stained with hematoxylin and eosin (H&E) and images captured with Axiophot microscope (Zelda). Femur X-ray scans were carried out using Faxitron MX20 (18 Kv, 10 s).

Hematologic parameters

Blood from non-transgenic controls and CD2-*Ostm1* transgenic mice were obtained by cardiac puncture and collected into EDTA-coated tubes (BD Microtainer). Haematological analysis was performed on a Bayer Advia 120 automated cell analyser with the mouse archetype of multispecies software version 2.206 (CBTR, Montreal, Canada).

Cell cultures

OP9 stromal cells expressing DL4 (Mohtashami et al., 2013) were plated at 2.0 × 10^4 cells/well and co-cultured with sorted gl/gl and control ETP cells (~500–750 cells). Cells were incubated in Opti-α-modified Eagle medium (OPTIMEM) supplemented with 50μM of 2-Mercaptoethanol (Sigma); 2 ng/mL of IL-7; 10 ng/mL Fms-like tyrosine kinase 3-ligand, 20 ng/mL of Stem Cell Factor (PeproTech) and 20% charcoal-stripped foetal bovine serum (Sigma). Frequency of cell distribution from co-cultures of DN1 to DP was determined by FACS analysis (day 5–20). Osteoclasts were generated and mature multinucleated osteoclasts identified by TRAP staining.

RNA sequencing

RNA was isolated from sorted DN1 thymic cell subset of +/+ NT, gl/gl and gl/gl TR with Magmax kit (Life technologies). RNA integrity and quality were assessed with Bionanalyzer RNA pico chips (Agilent). Ribosomal RNA depletion was carried out with an Epicentre kit followed by purification with RNA clean-up beads. Generation of transcriptome libraries from 4 to 25 ng of RNA using TruSeq stranded Kit protocol as well as Illumina protocol and reagents. Quality and quantity were evaluated with Nanodrop and HSdna chip. Samples were pooled and amplified in cDNA clusters using cBot (Illumina). Paired-end sequencing (PE50) was performed on HiSeq 2000. The RNA seq data reported herein have been deposited in the Gene Expression Omnibus (GEO) database under accession number GSE72184.

Computational analysis

Data reads were in FASTQ format. Gene expression analysis was performed (Trapnell et al., 2012). The bigWig files were generated from BAM files using UCSC gene browser alignment. Differential gene expression was established using Cuffdiff 2.2.1. Data were processed and presented using CummeRbund 2.6.1 with R 3.1.0 Analysis of biological and pathway changes corresponding to differentially expressed genes determined by computational tools using Ingenuity Pathway Analysis (IPA); Database for Annotation Visualization and Integrated Discovery (DAVID) and Gene Set Enrichment Analysis (GSEA).

QUANTIFICATION AND STATISTICAL ANALYSIS

Data are presented as means $\pm$ SEM. Statistical analysis was performed with Graphpad Prism software (San Diego, CA). Unpaired two-sample Student's t test evaluated statistical significance with $p < 0.05$.